9-21-2022

Mechanistic insight into functionally different human islet polypeptide (hIAPP) amyloid: the intrinsic role of the C-terminal structural motifs

Dibakar Sarkar

Narayan Chandra Maity

Gourav Shome

Kyriakos Gabriel Varnava

Vijayalekshmi Sarojini

See next page for additional authors

Recommended Citation

Sarkar, D., Maity, N. C., Shome, G., Varnava, K. G., Sarojini, V., Vivekanandan, S., Sahoo, N., Kumar, S., Mandal, A. K., Biswas, R., & Bhunia, A. (2022). Mechanistic insight into functionally different human islet polypeptide (hIAPP) amyloid: the intrinsic role of the C-terminal structural motifs. Physical chemistry chemical physics : PCCP, 24(36), 22250–22262. https://doi.org/10.1039/d2cp01650h

HHS Public Access

Author manuscript

Phys Chem Chem Phys. Author manuscript; available in PMC 2022 October 30.

Published in final edited form as:

Phys Chem Chem Phys. ; 24(36): 22250–22262. doi:10.1039/d2cp01650h.

Mechanistic insight into functionally different human islet polypeptide (hIAPP) amyloid: the intrinsic role of the C-terminal structural motifs†

Dibakar Sarkar[a], **Narayan Chandra Maity**[b], **Gourav Shome**[c], **Kyriakos Gabriel Varnava**[d], **Vijayalekshmi Sarojini**[d], **Subramanian Vivekanandan**[e], **Nirakar Sahoo**[f], **Sourav Kumar**[a], **Atin Kumar Mandal**[c], **Ranjit Biswas**[b], **Anirban Bhunia**[a]

[a]Department of Biophysics, Bose Institute, EN 80, Sector V, Kolkata 700 091, India.

[b]Chemical, Biological and Macromolecular Sciences, S. N. Bose National Centre for Basic Sciences, Sector-III, Salt Lake, Kolkata 700106, India

[c]Division of Molecular Medicine, Bose Institute, EN 80, Sector V, Kolkata 700 091, India

[d]School of Chemical Sciences, The University of Auckland, Private Bag 92019, Auckland, New Zealand

[e]College of Pharmacy, University of Kentucky, Lexington, KY 40536-0596, USA

[f]Department of Biology, University of Texas Rio Grande Valley, Edinburg, Texas, 78539, USA

Abstract

Targeting amyloidosis requires high-resolution insight into the underlying mechanisms of amyloid aggregation. The sequence-specific intrinsic properties of a peptide or protein largely govern the amyloidogenic propensity. Thus, it is essential to delineate the structural motifs that define the subsequent downstream amyloidogenic cascade of events. Additionally, it is important to understand the role played by extrinsic factors, such as temperature or sample agitation, in modulating the overall energy barrier that prompts divergent nucleation events. Consequently, these changes can affect the fibrillation kinetics, resulting in structurally and functionally distinct amyloidogenic conformers associated with disease pathogenesis. Here, we have focused on human Islet Polypeptide (hIAPP) amyloidogenesis for the full-length peptide along with its N- and C-terminal fragments, under different temperatures and sample agitation conditions. This helped us to gain a comprehensive understanding of the intrinsic role of specific functional

†Electronic supplementary information (ESI) available: ThT fluorescence parameters at different temperature (Tables S1 and S2); time-resolved fluorescence parameters (Tables S3-S5); activation energy determination from aggregation kinetics at different temperature (Fig. S1); time-resolved ThT fluorescence of hIAPP, VY21 and equimolar mixture (Fig. S2); Fitting of hIAPP aggregation kinetics using Amylofit (Fig. S3); ThT assay of co-incubated samples at different ratios (Fig. S4); SEM images of hIAPP, VY21 and equimolar mixture (Fig. S5). See DOI: https://doi.org/10.1039/d2cp01650h

bhunia@jcbose.ac.in, anirbanbhunia@gmail.com.

Author contributions

AB conceived, designed and executed the research; DS, NCM, SK and KGV performed the experiments; DS, NCM, VS, SV, RB, SK, NS, AKM and AB analyzed the results; DS and AB wrote the manuscript; all authors reviewed the manuscript; NS and AB arranged funding for this work.

Conflicts of interest

The authors declare no competing financial interests.

epitopes in the primary structure of the peptide that regulates amyloidogenesis and subsequent cytotoxicity. Intriguingly, our study involving an array of biophysical experiments and *ex vivo* data suggests a direct influence of external changes on the C-terminal fibrillating sequence. Furthermore, the observations indicate a possible collaborative role of this segment in nucleating hIAPP amyloidogenesis in a physiological scenario, thus making it a potential target for future therapeutic interventions.

1. Introduction

Protein misfolding and subsequent amyloid formation is allied with the pathology of a wide range of human diseases, including Alzheimer's, Parkinson's, type-2 diabetes, Huntington's disease, *etc*.[1-5] Human islet amyloid polypeptide (hIAPP) is a 37-residue peptide implicated in type-2 diabetes resulting from aggregation under certain conditions.[6,7] With regards to the growing prevalence of diabetes worldwide, it is increasingly important to gain mechanistic insight into hIAPP amyloidosis.[8-13] For a comprehensive understanding of the mechanism of hIAPP aggregation, it is imperative to consider the aggregation-prone domains within the hIAPP sequence. Over the years, emphasis has been given to discovering the residues crucial for hIAPP fibrillation. For example, the N-terminal $hIAPP_{8–16}$ fragment has been found to form fibrils with similar properties to hIAPP where Phe15 is required for stabilizing an on-pathway α-helical dimer.[14,15] Recent studies have revealed a crucial region spanning the residue stretch, $L_{12}ANFLVH_{18}$ associated with hIAPP aggregation.[14,16] Despite the fact that this segment does not directly partake in amyloidogenesis, it was found to interact with hIAPP and strongly enhance the β-sheet transition and fibril formation.[17] Several other small fragments of hIAPP have also been reported to form amyloids.[18] The $hIAPP_{20–29}$ fragment has been exclusively reported to form amyloid fibrils *in vitro* as well as play a significant role in amyloid formation.[19-21] However, the toxicity of this fragment was found to be considerably lower than that of the full-length peptide regardless of the strong tendency to form amyloid fibrils. The C-terminal segment harboring the $N_{22}FGAIL_{27}$ sequence has been extensively reported and studied for understanding the mechanisms of amyloidogenesis.[21-24] GxxxS/SxxxG motif present in this terminus is similar to the GxxxG repeating sequence in Amyloid β, which has been suggested to act as a modulator of fibrillation.[25] This segment has been shown to have a greater fibrillation propensity by several groups over the years. Recently, the C-termini of hIAPP oligomers were found to penetrate deeper into the lipid bilayer of the disordered domain.[26] The fact that the $hIAPP_{17–37}$ peptide was previously identified as one of the minor component in the human pancreas, has made it further intriguing in delineating the direct role of this peptide fragment in modulating the overall aggregation propensity of hIAPP.[27] Undoubtedly, peptide fragments have been useful in streamlining the analysis of the complex aggregation process. Knowledge of the primary sequence of the peptide is essential in determining its intrinsic propensity to undergo subsequently structurally and functionally distinct conformers in the amyloidogenesis cascade.

Apart from the intrinsic susceptibility of specific peptide segments, several external factors have been found to highly influence the aggregation process.[28] A change in such conditions may alter the aggregation mechanism and result in either amyloid or

disordered amorphous aggregates.[29] Over the years, the effect of peptide concentration, solvent pH, temperature, agitation, and ionic strength has been extensively studied.[30-33] Among them, temperature-dependent aggregation kinetics and agitation in the form of a magnetic stirrer or shaker table have been routinely used in studies of peptide and protein aggregation.[25,34] Temperature variation may alter the frequency of molecular collisions and affect intermolecular hydrophobic interactions, a major force in controlling aggregation.[35,36] Thus, the investigation of the temperature dependence of the aggregation process of a protein/peptide can be a suitable method to clarify the mechanisms leading to different kinds of aggregates.[37,38] Agitation on the other hand, has been employed so as to accelerate otherwise slow aggregation kinetics. While some found deviations in aggregation rate and structure, others showed that not agitation but the liquid–air or liquid–solid interface serve as the main culprit.[39-41] Despite the frequent use, little is understood about the impact of agitation on the aggregation nucleation process.

In this study, we undertook a systematic approach to gain high-resolution insight into the intrinsic and extrinsic factors involved in hIAPP amyloidosis. For this purpose, we compared the aggregation kinetics of hIAPP along with its N-terminal 18 residue peptide fragment KH18 (K_1-H_{18}) comprising the L_{12}ANFLVH_{18} sequence and the C-terminal 21 residue peptide VY21 (V_{17}-Y_{37}) harbouring the core N_{22}FGAIL_{27} fibrillating sequence as well as GxxxS/SxxxG motif (Fig. 1(A)) in different temperature and agitation conditions. This enabled us to gain a comprehensive understanding of hIAPP amyloidogenesis and subsequent toxicity in progressive pathogenesis. Further, our biophysical studies suggested a possible cooperative interaction of the specific fragments in seeding the overall pathogenesis.

2. Experimental methods

2.1. Sample preparation

Lyophilized synthetic peptides hIAPP and KH18 were purchased from Genscript Inc. USA and VY21 was synthesized using Fmoc protocols as previously published.[42] Briefly, the peptide was assembled on 2-chlorotrityl chloride resin (0.2 mmol scale) as C-terminal acid. Excess of each amino acid (4×), 3.9 equivalents of coupling reagent (HCTU) and OxymaPure® (3.9 equiv.) as suppressor of racemization were used. *N,N*-Diisopropylethylamine (DIPEA) was used as the base for couplings. Fmoc deprotection was performed using 20% piperidine in DMF. Cleavage from the resin was done using 10 mL of the trifluoroacetic acid (TFA) cocktail mixture (TFA–TIS–H_2O – 95 :2.5 : 2.5 v/v) per gram of the resin. TFA was evaporated and the crude peptide was precipitated using diethyl ether. The crude peptide was subsequently lyophilized and purified using reversed-phase high performance liquid chromatography (RP-HPLC) on a GE Pharmacia ÄKTA purifier 10 system or Thermo Scientific Dionex VWD 3 × 00 system using a Phenomenex Luna 5 μm C_{18} 100 Å (250 mm × 10 mm) column. Solvent A was 0.1% TFA in water and solvent B was 0.1% TFA and 0.09% water in 99% acetonitrile and the flow rate was 10 mL per min. The peptide was purified to >95% purity as shown by the analytical RP-HPLC trace on a Phenomenex Luna 5 μm C_{18} 100 Å (250 mm × 4.6 mm) column using the same solvent system as above at a flow rate of 1 mL per min. Matrix assisted laser desorption/

ionisation – time of flight mass spectrometry (MALDI-TOF MS) recorded on a Bruker Ultraftlextreme MALDI/TOF was used to characterize the peptide. 1 mg peptides were weighed and dissolved in 500 μL 1,1,1,3,3,3-hexafluoro-2-propanol (HFIP; Sigma-Aldrich, USA) and kept for 40 mins at 4 °C and then separated into 10 aliquots. The aliquots were lyophilized for 48 h and stored at −20 °C for further use.

2.2. Thioflavin T (ThT) fluorescence assay

Stock solutions of ~80 μM hIAPP, KH18, and VY21 peptides were prepared in a buffer containing 20 mM phosphate buffer (pH 7.3, 0.01% sodium azide) and 50 mM NaCl. Then the sample solutions were vortexed well, followed by a three-minute ultra-sonication and incubated at 25 °C or 37 °C temperature under shaking conditions. At various time-points, aliquots of peptides from incubations were taken and diluted to 10 μM final concentration, followed by the addition of 20 μM ThT for fluorescence intensity measurement. Fluorescence measurements were carried out using Hitachi F-7000 FL spectrometer with 240 nm min^{-1} scan speed. The excitation wavelength was kept at 440 nm and the emission range used was 460–520 nm, with 5 nm slit width for both the excitation and emission.

Further, peptide aggregation was studied under non-shaking conditions at different temperatures. 20 μM ThT was added into the sample solutions and ThT fluorescence was monitored under controlled temperatures using BMG LABTECH POLARstar Omega spectrometer in a 96 well plate.

Time-dependent ThT fluorescence data were fitted to a sigmoidal growth model:

$$Y = Y_0 + (Y_{\max} - Y_0) / (1 + \exp(t - t_{1/2} / b)) \quad (1)$$

Where the half-life $t_{1/2}$ is the time required to reach half of the fluorescence intensity, b is the apparent first-order constant and $Y_{\max}$, and Y_0 are, respectively, the maximum and initial fluorescence values.

The lag-time (t_{lag}) of amyloid kinetics was determined as ($t_{1/2} - 2b$).

Three independent experiments were performed throughout. All buffer solutions were filtered by using a 0.2 μm filter.

2.3. MTT assay

Cell culture and Cell viability assay.—RIN-5f cells derived from rat pancreatic β-cells were obtained from National Centre for Cell Science (NCCS, India) and maintained in complete RPMI-1640 media (Gibco) supplemented with 10% FBS, 1 unit per mL penicillin-streptomycin, 50 μg per mL gentamycin, and 2.5 μg per mL^{-1} amphotericin B at 37 °C in a humidified 5% CO_2 incubator. Experiments were carried out at 70–80% confluency.

Cell viability was measured using 3-(4,5-dimethylthiazol-2-yl)-2,5-diphenyltetrazolium bromide (MTT), which reflects the mitochondrial activity of living cells. Viable cells were able to reduce MTT into purple formazan by mitochondrial enzyme; and the amount of

formazan formation indicates cell viability. Briefly, 1×10^4 cells per well were seeded in 96-well plate for 24 h. Cells were then treated with 10 μM of each hIAPP, KH18 and VY21 peptides taken out at various time-points (0, 10, 60 and 240 min) in shaking conditions. In addition, RIN-5f cells were also treated with 10 μM of hIAPP, KH18, VY21 and hIAPP + VY21 (1 : 1 molar ratio) peptides which were taken at various time-points (0, 2, 5, and 24 h) in non-shaking conditions. After 24 h of treatment, MTT was added to the wells at a final concentration of 0.5 mg mL^{-1} and incubated at 37 °C and 5% CO_2 humidified incubator for another 3.5 h. 100 μL of dimethyl-sulfoxide (DMSO) was added to each well to dissolve the formazan precipitate. The absorbance was taken at 570 nm using a microplate reader. Results were expressed as a percentage of control.

2.4. Circular dichroism (CD) spectroscopy

CD measurements were taken on a JASCO J-1500 CD spectrometer using a 0.1 cm path length cell with a slit width of 2 nm. Peptides of ~80 μM concentration were prepared in 20 mM phosphate buffer, 50 mM NaF (pH 7.3), and incubated at 37 °C under shaking conditions as well as at 25 °C under non-shaking conditions. At different time intervals, Far-UV CD spectra were recorded at 20 °C, from 260 nm to 190 nm, with a scan speed of 100 nm min^{-1}. For each spectrum, three readings were taken (*i.e.*, three accumulations), and the average was considered. Smoothing and buffer subtraction were done to process raw data, as per the manufacturer's recommendation.

2.5. Time-resolved fluorescence assay

Time-resolved fluorescence (TRF) experiments were performed *via* time-correlated single-photon counting (TCSPC, LifeSpecps, Edinburgh Instrument, U.K.) technique.[43] All TRF samples were excited with 409 nm wavelength LED laser. The scattering solution was excited at 409 nm, and the emission was also collected at 409 nm with the magic angle orientation of the emission polarizer with respect to excitation, and the instrument response function (IRF) was collected. The full-width half maxima (FWHM) of IRF was 85 ps. The TRF emission of ThT in these experiments was collected at 485 nm. The average excited-state lifetime $\langle \tau_{life} \rangle$ of ThT was calculated from the magic angle TRF decay collected at the emission peak wavelength of ThT in these samples considering the formula $\langle \tau_{life} \rangle = \sum_i a_i \tau_i$, where $\sum_i a_i = 1$. The TRF samples were prepared by mixing the required amount of hIAPP, VY21, and their 1 : 1 mixture (80 μM) in the buffer mentioned above containing 20 μM ThT. All TRF measurements were performed for up to 6 h at 25 °C. The isothermal condition was made by using the Julabo temperature controller (accuracy ±1 K).

2.6. Nuclear magnetic resonance spectroscopy

The lyophilized samples were re-suspended in 20 mM sodium phosphate, 50 mM NaCl (pH 7.3). All NMR samples were prepared in sodium phosphate buffer containing 10% deuterated water (v/v). ^1H NMR spectra were obtained using 128 scans with a recycle delay of 1.5 s. All NMR experiments were carried out on a 500 MHz Bruker spectrometer equipped with RT probe at 25 °C. All NMR spectra were processed using Topspin™ 4.0.6 (Bruker software suite).

2.7. Transmission electron microscopy (TEM)

TEM sample preparation was done by diluting the stock solution into 10 μM for each variant in Milli-Q water. Then 10 μL of each sample was spotted on a carbon-coated copper grid (Electron Microscopy Sciences, USA), followed by an incubation of 30 minutes. It was subsequently followed by washing with Milli Q water and staining with freshly prepared filtered 1% (w/v) uranyl acetate solution (Electron Microscopy Sciences, USA) for 5 minutes. Finally, samples were air-dried for 30 minutes. Imaging was done using a transmission electron microscope FEI Tecnai TF20 at 200 kV with a point resolution of 0.24 nm and line resolution of 0.102 nm. Recording of images was done digitally, and analysis was done in EDS mode.

2.8. Scanning electron microscopy (SEM)

Aliquots of each peptide solution were taken at the saturation phase and deposited on a glass slide, followed by overnight air-drying. The slides were then coated with gold for 120 s at 10 kV voltage and 10 mA current. The sample images were recorded using a ZEISS EVO-MA 10 scanning electron microscope equipped with a tungsten filament gun operating at 10 kV.

3. Results

3.1. Fibrillation kinetics of hIAPP, KH18, and VY21

We first compared the aggregation kinetics of hIAPP, KH18 (K_1–H_{18}), and VY21 (V_{17}–Y_{37}) (Fig. 1(A)) using Thioflavin T (ThT) dye[44,45] at physiological pH, but, at different temperatures. Under shaking conditions (250 rpm) at 37 °C, hIAPP displayed a rapid aggregation profile. VY21, the C-terminal fragment, on the other hand, showed slower aggregation kinetics, while the N-terminal, KH18, did not induce any increase in the ThT fluorescence intensity over the experimental time-frame. The respective time-dependent kinetic curves were fitted with a sigmoidal growth model to determine the corresponding half-time ($t_{1/2}$) and lag-time (t_{lag}) of the aggregation kinetics (Fig. 1(B)).[46] At the given temperature and shaking conditions, hIAPP exhibited no t_{lag}, reaching $t_{1/2}$ within just 8.45 ± 1.07 min of incubation. While KH18 did not show any aggregation, VY21 displayed a sigmoidal growth kinetics with a t_{lag} of 18.40 ± 1.60 min and a $t_{1/2}$ of 50.85 ± 1.77 min (Table S1, ESI†). Having this distinct difference in the overall aggregation propensities between the peptides, we measured their corresponding fibrillar cytotoxicity to correlate their pathogenic propensity (Fig. 1(C)).

3.2. Cytotoxicity of amyloid fibrils formed at 37 °C, under shaking conditions

To compare the cytotoxic effects of fibrilar/oligomeric hIAPP with the fragment peptides generated at 37 °C, under shaking conditions (250 rpm), we performed MTT reduction assay with RIN-5F cells using 3-(4,5-dimethylthiazol-2-yl)2,5-diphenyltetrazolium bromide (MTT) dye reduction as an indicator of good metabolic health.[47] RIN-5F insulinoma cells,

†Electronic supplementary information (ESI) available: ThT fluorescence parameters at different temperature (Tables S1 and S2); time-resolved fluorescence parameters (Tables S3-S5); activation energy determination from aggregation kinetics at different temperature (Fig. S1); time-resolved ThT fluorescence of hIAPP, VY21 and equimolar mixture (Fig. S2); Fitting of hIAPP aggregation kinetics using Amylofit (Fig. S3); ThT assay of co-incubated samples at different ratios (Fig. S4); SEM images of hIAPP, VY21 and equimolar mixture (Fig. S5). See DOI: https://doi.org/10.1039/d2cp01650h

which closely resemble pancreatic β-cells, were chosen as an *ex vivo* model system to measure the cytotoxicity of the respective peptides whose effects are more pronounced in the pancreas and closely represent type II diabetes pathology. Fig. 1(C) shows that hIAPP preparations containing amyloid fibrils/oligomers are significantly more toxic than either KH18 or VY21 as compared to untreated control. Incubating the cells with hIAPP at different time-points of 0 min, 10 min, 60 min, and 240 min reduces the viability to 32%, 44%, 13%, and 20%, respectively as compared to the controls. Correlating with the ThT fluorescence, we observed a correlation between the aggregated states and cytotoxicity. Samples at 0 min and 10 min, which largely contain oligomers are highly toxic. On the other hand, the cell viability increased with the predominance of growing protofibrils and mature fibrillar species (samples at 60 min and 240 min, respectively). The non-aggregating KH18 peptide fragment was found to be non-toxic at the aforesaid time points. Similarly, VY21 did not show any toxicity at 0, 10 or 60 min time points. However, only slight reduction in cell viability was observed at 240 min. Thus, despite the ThT-positive aggregates, VY21 amyloid aggregates were less toxic to the RIN-5F cells. This suggested that the intrinsic amyloidogenic propensity of the full-length or C-terminal fragment cannot directly correlate to the functional attributes of the eventual conformers. Probably, some other factors might be dictating much of the functional pathogenesis. This prompted us to extend our studies into understanding the direct role played by the extrinsic factors.

3.3. Effect of temperature on aggregation kinetics

The very fast aggregation kinetics of hIAPP and VY21 at 37 °C, under shaking conditions, made it difficult to distinctively correlate the cytotoxicity with the aggregated species. Small temperature variations can significantly impact the protein folding and may cause non-native aggregation.[28] Thus, modulating the experimental temperature might help regulate the overall aggregation rate for a better structural insight into the functional toxicity. Here, we investigated the aggregation kinetics of the peptide variants at a lower temperature (25 °C) while keeping the shaking conditions (250 rpm) the same (Fig. 1(D)). Consequently, an increased t_{lag} of 8.41 ± 2.10 min and 61.78 ± 18.54 min was detected at 25° temperature for hIAPP and VY21, respectively. Similarly, the $t_{1/2}$ value for hIAPP and VY21 was found to be 31.73 ± 2.14 min and 109.72 ± 18.94 min, respectively (Table S2, ESI†). Thus, lowering the temperature reduced the aggregation rates for both hIAPP and VY21.

3.4. Aggregation kinetics under quiescent conditions

Studies have shown that agitation may induce protein/peptide aggregation.[48] Therefore, in order to examine the influence of agitation on the aggregation kinetics, we performed a ThT fluorescence assay under quiescent conditions at different temperatures. At 25 °C, hIAPP displayed a typical sigmoidal growth curve of amyloid formation. The fluorescence intensity started to increase gradually after a lag-time of 160.70 ± 2.00 min, reached $t_{1/2}$ at 210.00 ± 1.00 min, and saturated at ~360 min of incubation (Fig. 2(A)). To gain mechanistic insights into the formation hIAPP fibrillation, we performed the global fitting of the ThT curves using the online platform AmyloFit[49] and obtained the rate constants for the individual microscopic steps. Different kinetic models were checked for fitting of the experimental data. Interestingly, we found that the models that do not include secondary nucleation failed to properly fit the experimental kinetic curve. The multi-step secondary nucleation model

best fitted the experimental data (Fig. S3, ESI†). In this model, peptide monomers first bind to the surface of the fibrils, which is monomer concentration-dependent. This is followed by monomer concentration-independent steps that could involve conformational rearrangement, the formation of a nucleus, and detachment from the surface of the fibrils. From the model fitting we obtained the rate constants k_+ (elongation rate constant), k_n (primary rate constant), k_2 (secondary nucleation rate constant) as well as the Michaelis constant K_M all of which were comparable to the previously reported data on hIAPP aggregation.[50] We also found that the combined rate constant for secondary nucleation, k_+k_2, is larger than the combined rate constant k_+k_n containing primary nucleation, such that $k_2/k_n > 10^8$, suggesting that most of the new aggregates are formed through surface-catalyzed secondary nucleation rather than through primary nucleation. Interestingly, VY21 displayed completely different aggregation kinetics. Despite the composite core fibrillating sequence, VY21 displayed considerable differences under quiescent conditions with very little increase in the ThT intensity compared to hIAPP. Due to the complex nature of oligomerization, we could not fit the data using the online platform Amylofit. KH18, on the other hand, did not show any aggregation whatsoever (Fig. 2(A)).

Interestingly, at a higher temperature (32 °C) under non-shaking conditions, hIAPP displayed a considerably faster aggregation with $t_{1/2}$ of 188.00 ± 3.40 min and t_{lag} of 100.00 ± 5.70 min (Fig. 2(B)). VY21 exhibited similar kinetics to that of 25 °C, which suggests that in order to undergo fibrillation, VY21 requires shaking. KH18, on the other hand, did not show any aggregation. Similarly, a further increase in the incubation temperature resulted in lowering of lag-time for hIAPP but did not affect the aggregation kinetics KH18 or VY21 substantially (Fig. 2(C)). At 37 °C, hIAPP displayed a t_{lag} of 82.00 ± 2.80 min, reaching $t_{1/2}$ at 138.00 ± 1.50 min of incubation. The fibrillation t_{lag} of hIAPP was plotted as a function of temperature, which suggested a drastic difference in the initial elongation rates (Fig. S1A, ESI†). The Arrhenius plot of initial elongation rates on a logarithmic scale vs. inverse temperature indicated data points well fitted ($R = 0.99$) with a straight line (Fig. S1B, ESI†). From the slope of the straight line, we calculated the activation energy, E_A to be 43.8 ± 5.6 kJ mol^{-1}, suggesting a significant conformation change associated with the addition of hIAPP monomer to the fibrils.[51]

Since the hIAPP sample in non-shaking conditions and at 25 °C resulted in a distinct observation of lag phase, we performed MTT assay to assess the cytotoxicity of the aggregated species. Fig. 2(D) clearly depicts the distinct effect of the different aggregated states of hIAPP on the survival rates of RIN-5F cells. Interestingly, when compared to the aggregation kinetics, we observed a strong connection between the time frame of lag phase (0–3 h) and the pronounced cytotoxicity detected for the hIAPP species. hIAPP sample at 2 h of incubation showed the most cytotoxic effect because of the predominant existence of the oligomers. As the nucleation and growth phase proceeds, a significant decrease in the toxicity was apparent. While the cells treated with the oligomers (sample obtained at 2 h) showed ~70% of survival, the growing protofibrils (collected at 5 h) resulted in ~90% cell viability. Interestingly, KH18 retained its non-toxic nature up to 5 h of incubation (no significant reduction of cell viability), with only 8% decrease in the cell viability observed for the sample collected at 24 h. Nonetheless, a possible explanation would be the generation of few low molecular weight oligomers, which may attribute to the

observed toxicity. When cells were incubated with an equimolar concentration of VY21 at different time-points of incubation, we found a slight reduction in the cell viability compared to the control. This is intriguing, as under the given conditions, the ThT assay indicated that VY21 remains mostly as oligomers. Thus, it is possible that the structural difference and the non-transient nature of these oligomeric species decide the difference in toxicity profile with hIAPP oligomers. Therefore, our experimental observations indicated only a direct correlation between cytotoxicity and aggregated state for hIAPP alone, supporting the “oligomer hypothesis” of amyloidosis. Neither VY21 nor KH18 displayed a profile that clearly correlates the toxicity and the aggregation state. Overall, these findings suggest that under non-shaking conditions, VY21 forms stable oligomers; however, it could not trigger substantial cellular death.

3.5. Secondary structure determination by CD spectroscopy

To compare the characteristic changes in the secondary conformation during aggregation, we performed Circular Dichroism (CD) spectroscopy at different time points of incubation (Fig. 3). Initially, hIAPP displayed α-helical conformation, with representative double minima near 206 nm and 222 nm (Fig. 3(A) and (B)). At 37 °C, under shaking conditions (250 rpm), the conformational transition to β-sheet occurred very rapidly (within 180 min). Within the same time interval, hIAPP showed negligible changes in the secondary structure when incubated at 25 °C under non-shaking conditions, suggesting a slower aggregation rate. Thus, the aggregation rates are highly dependent on the external factors, correlating well with the ThT assay. However, the overall population of the intermediate toxic oligomers retained their helical conformation, preventing further characterization from the CD spectra. Similarly, the toxic hIAPP fibrils generated under different aggregation conditions manifested in β-sheet secondary conformations. Fig. 3(C) and (D) indicates that KH18 did not show noticeable changes in the CD spectra within the experimental time under both experimental conditions. Overall, the non-toxic KH18 exhibited double minima near 206 nm and 222 nm, representing α-helical conformation, and remained unchanged throughout the experiment. Surprisingly, the VY21 fibrils formed under shaking conditions (250 rpm) at 37 °C, which are non-toxic in nature, have β-sheet secondary conformation (Fig. 3(E)). Under the given conditions, we observed a swift change from the random coil (minima at 196 nm) to β-sheet fibrils. Under non-shaking conditions, the percentage of random coil decreased with time; however, no visible β-sheet conformation was observed in the CD spectra, corroborating well with the ThT data (Fig. 3(F)). Thus, the less-toxic VY21 aggregates have predominantly disordered secondary conformation.

3.6. Time-resolved fluorescence (TRF) of ThT provides a better understanding of fibril formation

In order to have a better understanding of the origin of the above-described fluorescence intensity variances between hIAPP and VY21, the fluorescence lifetime of ThT molecules during the aggregation process was measured by Time-resolved fluorescence (TRF) emission decay, collected at the emission polarizer’s magic angle orientation at 25 °C temperature under non-shaking conditions (Fig. 4). The lifetime emission decay was fitted to a sum of three exponential functions of time, and the average lifetime $\langle \tau_{life} \rangle$ was obtained *via* time integration of the fit parameters. Earlier femtosecond up-conversion

experiments reported tri-exponential ThT fluorescence intensity decay in bulk water.[52] On the other hand, bi-exponential or multi-exponential fluorescence lifetime decays of ThT in normal high viscous solvents, binary mixtures and in amyloid fibril systems have been reported by detection systems with temporal resolutions of a few tens of picosecond.[52-54] The multi-exponential ThT intensity decay kinetics, measured by us in this work, is, therefore, a reflection of the inherent multi-exponential character of ThT fluorescence lifetime decay. We have found that the fluorescence lifetime of ThT corroborated well with the ThT fluorescence kinetic assay (Fig. 2(A)). Note that the average lifetime of ThT did not increase considerably during the lag time of hIAPP aggregation. After ~180 min of incubation, the lifetime of ThT gradually increased due to oligomerization and subsequent amyloid formation. In contrast, the ThT lifetime kinetics in the presence of VY21 showed no lag-time; however, it did not increase much compared to hIAPP. The lifetime of ThT largely depends on the torsional restriction between benzothiazole moiety and the amino benzene ring. Thus, ThT lifetime can increase if the torsional restriction imposed by molecular friction is enhanced through either solvent viscosity,[53,55] medium confinement[56] or incorporation of ThT inside β-sheets.[52] CD spectra of VY21 under non-shaking condition (Fig. 3(F)) indicates that aggregation of VY21 in aqueous solution dose not lead to formation of β-sheet during incubation period. It is noteworthy to mention that the steady state fluorescence intensity (I_{ss}^{f}) depends non-linearly on radiative (K_r) and non-radiative (K_{nr}) rates via the relation,[57] $I_{ss}^{f} = \varphi_f I_0(1 - 10^{-A})$, where $\varphi_f = K_r/(K_r + K_{nr})$. φ_f denotes quantum yield, I_0 and A are intensity of incident light and absorbance respectively. Average fluorescence lifetime, on the other hand depends on K_r and K_{nr} as follows: $\langle \tau_{life} \rangle = 1/(K_r + K_{nr})$. As the aggregation proceeds, ThT experiences increasing restriction on its torsional mode during twisted intramolecular charge transfer (TICT) under photo-excitation. This in turn decreases K_{nr} and lengthens average lifetime $\langle \tau_{life} \rangle$. Although I_{ss}^{f} and $\langle \tau_{life} \rangle$ depends on K_r and K_{nr} of ThT, the connecting relations are not the same. The small increase of I_{ss}^{f} in the beginning of the incubation period and the relatively weaker increase of the $\langle \tau_{life} \rangle$ during the same time therefor suggest that ThT experienced somewhat restricted environment due to VY21 aggregation. The absence of β-sheets in VY21, on the other hand, resulted in a shorter lifetime $\langle \tau_{life} \rangle$ of ThT compared to that in the case of hIAPP, because of the relatively less frictional resistance on ThT torsional mode. The time-dependent changes in the intensity decay amplitudes (a_1, a_2, and a_3) of the respective samples suggest that progressive formation of β-sheets followed by amyloid formation increases the local friction, which, in turn, increases the population with longer lifetimes (Fig. S2, ESI†). With time, the decrease of ‘free’ ThT molecules and the simultaneous increase of the ‘bound’ ThT molecules leads to lengthening of the average fluorescence lifetime. ThT molecules located in disorder oligomeric environments or inside β-sheet channels in fibril, naturally experiences enhanced frictional resistance and contributes to the lengthening of the average fluorescence lifetime of ThT in peptide aggregations shown in the present measurements.

3.7. Insights from NMR spectroscopy

We next performed solution state ^{1}H NMR spectroscopy to monitor the kinetics of monomer loss, and detect soluble intermediate species. Time-dependent one-dimensional (1D) NMR spectroscopy has often been used to detect the intensity drop of the peptides during

aggregation for its advantage of not requiring any external fluorophore like ThT (Fig. 5(A)-(C)).[58] The signal intensity of the amide peaks for each peptide was measured at 25 °C under non-shaking conditions and plotted as a function of time intensity (Fig. 5(D)). hIAPP exhibited a gradual decrease in the monomer concentration and showed ~80% decay in the signal intensity at the time of saturation. Apart from the line broadening no new peaks appeared in the 1D spectra during the experimental time-frame. The kinetics of hIAPP measured by NMR tend to be slower than that observed by ThT fluorescence. It can be attributed to interface effects with the container well and air–water interface that are different between NMR tubes and 96-well plates.[59] Also, the absence of ThT molecules can slightly affect the kinetics of aggregation.[60] KH18 displayed negligible decrease in the NMR signal intensity throughout the experimental time. In case of VY21, the most striking changes occurred within just 60 min of incubation. There is a 30% drop in the overall amide peak intensity within that time and then the system gradually stabilized with a final decay of ~40% signal intensity. Thus while a significant decrease in the VY21 amide peak intensity occurs immediately after dissolution that plateaus at around 60 min, a slower sigmoidal type transition for hIAPP was apparent. The time-dependent NMR kinetics suggests that the rate of oligomerization in VY21 is much higher than that of hIAPP. However, the VY21 oligomeric intermediates remains stable unlike hIAPP, which gradually converts into amyloid fibrils within the same experimental time frame.

3.8. The C-terminus of hIAPP acts as an enhancer of aggregation

We further examined the effect of VY21 on hIAPP under the same non-shaking conditions. Studying such interaction has also been proven to be effective in developing inhibitory agents for both Aβ and hIAPP.[61-64] We co-incubated hIAPP and VY21 at a 1 : 1 molar ratio and measured the time-dependent ThT fluorescence intensity. Interestingly, we observed an initial increase in the ThT intensity with no lag time, suggesting a rapid oligomerization (Fig. 6(A)). Possibly, VY21 interacted with the full-length hIAPP and interfered with the hIAPP amyloid formation. Even when added in substoichiometric concentration, VY21 accelerates the hIAPP assembly significantly. Upon increasing the concentration of VY21, a clear decrease in the lag-phase of hIAPP was observed, which signifies the dose-dependency on hIAPP aggregation (Fig. S4, ESI†). Further, VY21 was incubated for 3 h in the presence of ThT, and the hIAPP monomer was then added to check the effect of oligomeric VY21 on the aggregation of hIAPP. As soon as the monomeric hIAPP was added, we observed an exponential increase in the ThT intensity, suggesting that VY21 aggregates act as a seed and drastically accelerate the aggregation process of hIAPP (Fig. 6(A)).

Co-incubation of hIAPP with VY21 at a 1 : 1 molar ratio is also reflected in the disappearance of lag-time of ThT lifetime kinetics as observed in TRF kinetics (Fig. 6(B)). We have already discussed the different dependencies of $\langle \tau_{life} \rangle$ and I_{ss}^{f} on K_r and K_{nr}. Because the dependencies of I_{ss}^{f} and $\langle \tau_{life} \rangle$ on K_r and K_{nr} are not the same, slightly different time profiles for $\langle \tau_{life} \rangle$ and I_{ss}^{f} are seen in Fig. 6(A) and (B). The rate of increase in the ThT lifetime was higher than hIAPP alone, suggesting a higher oligomerization rate of hIAPP in the presence of VY21. The saturation time of ThT lifetime in the co-incubated sample also reached earlier than hIAPP alone. However, the saturating lifetime value was slightly

less than that of hIAPP, suggesting a difference in the aggregate structure or size. VY21 thus primarily promotes oligomerization but leads to alteration of mature fibril formation. The average lifetime $\langle \tau_{life} \rangle$ of ThT in hIAPP or the equimolar mixture (hIAPP : VY21 = 1 : 1) indicates that the formation of β-sheet during aggregation of hIAPP alone ($\langle \tau_{life} \rangle_{ThT}$ ~ 776 ps) is more pronounced than that in the equimolar mixture ($\langle \tau_{llfe} \rangle_{ThT}$ ~ 597 ps).

The effect of VY21 on the aggregation of hIAPP was also monitored by NMR spectroscopy. The monomer depletion plot showed that VY21 induced a sigmoidal decay curve with a higher rate and ~70% decay of signal intensity at the time of saturation (Fig. 6(C)). Unlike ThT assay, NMR data showed that monomer intensity decrease is comparatively slow in the initial phase for both hIAPP and Co-incubated sample. This may appear to be a lag. However, this ‘lag’ period is not real because the NMR intensity does decrease with time but at a rate slower than that found in fluorescence measurements. This can be ascribed to interface effects with the container well and air, as well as the influence of ThT as described previously. Qualitatively, however, the NMR data showed similar kinetic profiles to that of ThT fluorescence kinetics. Both data suggested that co-incubation with VY21 greatly influenced the aggregation kinetics of hIAPP.

MTT assay was also performed for the assessment of cytotoxicity of the co-incubated sample at different time points of aggregation. Interestingly, the toxicity profile of the mixed sample at different time points showed significantly reduced cell death as compared to hIAPP alone (Fig. 6(D)). The effect of VY21 on the hIAPP pathogenesis was profound only in the 2 h sample, where the cell viability reduced to 18%. This may be attributed to free hIAPP oligomers still present in the sample solution. Interestingly, at later stages, collected at 5 h and 24 h (similar to hIAPP alone for comparison, Fig. 2(D)) of aggregation, where growing protofibrils and fibrils are predominant, we observed almost no cytotoxicity (94–99% cell viability). Thus, VY21 alters the overall fibrillation pathway reducing the concentration of toxic soluble prefibrillar species. Taken together, these findings suggest that under non-shaking conditions at 25 °C, VY21 amplified the rate of fibrillation drastically, playing a rather protective role.

3.9. Morphology of aggregated species

Next, we attempted to visualize the morphology of the aggregates generated at 25 °C under non-shaking conditions by employing high-resolution electron microscopy. An array of microscopic imaging was executed to determine the morphological characteristics of the aggregates under examination. Scanning Electron Microscope (SEM) image confirmed that hIAPP forms amyloid both in the absence and presence of VY21, while VY21 alone did not (Fig. S5, ESI†). High-resolution Transmission Electron Microscope (TEM) images revealed the presence of hIAPP aggregates with an average width of ~110 ± 43 nm (Fig. 6(E)). In contrast, VY21 aggregates were amorphous with few spherical structures with a 203 ± 20 nm diameter (Fig. 6(F)). Interestingly, when co-incubated with VY21, the overall fibril density of hIAPP aggregates was less than the hIAPP alone, with an average width of 84 ± 14 nm (Fig. 6(G)).

4. Discussion

Studying peptide fragments have been promising in understanding the differential behaviour of the full-length peptide, as different regions of an aggregating peptide may be involved in different structural and functional attributes.[65,66] Previously, Brender *et al.* showed that the N-terminal $hIAPP_{1–19}$ fragment could disrupt synthetic lipid vesicles to a similar extent as the full-length hIAPP peptide without forming amyloid fibers.[67] Our results also indicate that the N-terminal KH18 fragment could not undergo fibrillation; this could possibly be due to the disulphide bond between the two cysteine residues at positions 2 and 7. This conformationally restricts the peptide to adopt β-sheet and may influence the overall propensity to form amyloid fibrils.[68] In contrast, both hIAPP and VY21 showed a time-dependent increase in ThT intensity. Differences in ThT intensity could possibly be either due to the number of ThT accommodations or the different affinity of the ThT binding sites or the difference in quantum yields.[69-71] The observed difference in ThT fluorescence lifetime between hIAPP and VY21 aggregates suggests that the ThT molecules bound to different aggregates do have different quantum yields.

Misfolding of proteins/peptides may lead to two primary forms of aberrant aggregates: ordered amyloid fibrils and disordered amorphous aggregates.[29,72] While studying the aggregation kinetics of individual peptides, we observed that for the same peptide, the fibrils formed under agitation differ greatly from those formed under quiescent conditions. Our observation showed that at physiological pH, VY21 could evolve through two distinct pathways, leading to the formation of either disordered or ordered amyloid aggregates. It preferentially forms disordered oligomers at low temperatures under non-shaking conditions, whereas agitation results in the ThT-positive amyloid fibrils. With respect to the disordered aggregates, the fibril formation requires higher conformational changes, and agitation serves that purpose. Although, amyloid oligomers have been extensively reported in the literature to impart much of the cytotoxicity when compared to the corresponding fibrillar species,[73-75] to our surprise, VY21 oligomers were not significantly toxic when compared to hIAPP. The disordered conformation of these oligomers (confirmed by CD spectroscopy) may result in reduced toxicity. Moreover, these can form potential seeds that can prompt a cascade of aggregation kinetics, where upon the peptide can either undergo conformational changes or induce changes in dynamic exchange with the monomeric species resulting in differential amyloidosis. Nevertheless, VY21 acts as a scavenger by drastically reducing the availability of toxic soluble hIAPP oligomers. Further, the less toxic oligomers of VY21 proved to be an antagonist of hIAPP oligomers since no lag phase was observed in the presence of such oligomers. This, in turn, suggests the shortening of lifetime for the toxic hIAPP oligomers. A recent study by Sheena E. Radford and co-workers also reported small molecule accelator of hIAPP aggregation.[50] However, there are very few studies of such kind. A comprehensive understanding of such accelerated aggregation by small molecules/peptides would pave the way for designing therapeutic inerventions in the field of amyloidosis.

Overall, our results indicate that the aggregation of VY21 is more complicated than simply a transition from random coil to β-sheet. It clearly has a diverse and intriguing free-energy landscape with multiple barriers, resulting in different kinds of aggregate and cytotoxicity. However, for full-length hIAPP peptides, the amyloid formation occurred irrespective of

temperature or agitation (Fig. 7). The results suggest that a high free energy barrier of nucleation is decided by the ordered structures of amyloid fibrils and that disordered aggregation occurs promiscuously without a high free energy barrier. The introduction of agitation may influence the conformational transitions of VY21, leading to the exposure of usually buried regions, such as hydrophobic groups. Thus new intermolecular interaction may come forward, regulating the aggregation process.

The formation of amyloid fibril and disordered aggregates from full-length hIAPP and its C-terminal segment encoded by the VY21 peptide fragment suggests a possible exciting collaboration between the two in the subsequent pathological aggregation propensity of hIAPP. Thus, the $N_{22}FGAIL_{27}$ sequence motif present in the C-terminal segment of hIAPP (VY21) may not be sufficient to undertake amyloid formation under quiescent conditions. The interaction between the C-terminal and the N-terminal segment may influence the aggregation pathway of full-length hIAPP under quiescent conditions.[76] This is interesting, given this alternatively suggests that prevention of this interaction might directly enable efficient therapeutic solution development. Moreover, the ability of VY21 oligomers to act as an enhancer of hIAPP aggregation while reducing overall cytotoxicity makes it a potential target for inhibitor designing.

5. Conclusion

We accentuated the significance of the VY21 peptide in generating structurally different oligomers. The introduction of agitation modifies the phase diagram dramatically, releasing the kinetic trap and establishing the equilibrium determined by the intrinsic solubility of VY21. Even though the disordered oligomers were structurally different, they act as templates for hIAPP, drastically accelerating the aggregation process while reducing the overall fibrillar toxicity. Our findings thus may assist in finding therapeutics based on the kinetic differences in the aggregation behavior.

Supplementary Material

Refer to Web version on PubMed Central for supplementary material.

Acknowledgements

DS acknowledge DST-INSPIRE (Government of India) for providing a Senior Research Fellowship. NCM acknowledges Council of Scientific and Industrial Research (CSIR), Government of India, for Senior Research Fellowships (SRF).

Funding sources

This work was partly supported by Department of Biotechnology (BT/PR29978/MED/30/2037/2018 to AB and AKM), Government of India and partly by Council of Scientific and Industrial Research (02(0292)/17/EMR-II to AB), Government of India and partly by NIH Grant, USA (SC2GM139715 to NS).

References

1. Chiti F and Dobson CM, Annu. Rev. Biochem, 2017, 86, 27–68. [PubMed: 28498720]
2. DeToma AS, Salamekh S, Ramamoorthy A and Lim MH, Chem. Soc. Rev, 2012, 41, 608–621. [PubMed: 21818468]

3. Mukherjee A, Morales-Scheihing D, Butler PC and Soto C, Trends Mol. Med, 2015, 21, 439–449. [PubMed: 25998900]
4. Zaman M, Khan AN, Wahiduzzaman M, Zakariya SM and Khan RH, Int. J. Biol. Macromol, 2019, 134, 1022–1037. [PubMed: 31128177]
5. Bolognesi B, Kumita JR, Barros TP, Esbjorner EK, Luheshi LM, Crowther DC, Wilson MR, Dobson CM, Favrin G and Yerbury JJ, ACS Chem. Biol, 2010, 5, 735–740. [PubMed: 20550130]
6. Cooper GJ, Willis AC, Clark A, Turner RC, Sim RB and Reid KB, Proc. Natl. Acad. Sci. U. S. A, 1987, 84, 8628–8632. [PubMed: 3317417]
7. Cao P, Marek P, Noor H, Patsalo V, Tu LH, Wang H, Abedini A and Raleigh DP, FEBS Lett., 2013, 587, 1106–1118. [PubMed: 23380070]
8. Raleigh D, Zhang X, Hastoy B and Clark A, J. Mol. Endocrinol, 2017, 59, R121–R140. [PubMed: 28811318]
9. Fernández MS, Cell Calcium, 2014, 56, 416–427. [PubMed: 25224501]
10. Bedrood S, Li Y, Isas JM, Hegde BG, Baxa U, Haworth IS and Langen R, J. Biol. Chem, 2012, 287, 5235–5241. [PubMed: 22187437]
11. Krotee P, Rodriguez JA, Sawaya MR, Cascio D, Reyes FE, Shi D, Hattne J, Nannenga BL, Oskarsson ME, Philipp S, Griner S, Jiang L, Glabe CG, Westermark GT, Gonen T and Eisenberg DS, eLife, 2017, 6, 19273.
12. Luca S, Yau WM, Leapman R and Tycko R, Biochemistry, 2007, 46, 13505–13522. [PubMed: 17979302]
13. Mascioni A, Porcelli F, Ilangovan U, Ramamoorthy A and Veglia G, Biopolymers, 2003, 69, 29–41. [PubMed: 12717720]
14. Louros NN, Tsiolaki PL, Zompra AA, Pappa EV, Magafa V, Pairas G, Cordopatis P, Cheimonidou C, Trougakos IP, Iconomidou VA and Hamodrakas SJ, Biopolymers, 2015, 104, 196–205. [PubMed: 25913357]
15. Wiltzius JJ, Sievers SA, Sawaya MR and Eisenberg D, Protein Sci., 2009, 18, 1521–1530. [PubMed: 19475663]
16. Jaikaran ET, Higham CE, Serpell LC, Zurdo J, Gross M, Clark A and Fraser PE, J. Mol. Biol, 2001, 308, 515–525. [PubMed: 11327784]
17. Scrocchi LA, Ha K, Chen Y, Wu L, Wang F and Fraser PE, J. Struct. Biol, 2003, 141, 218–227. [PubMed: 12648568]
18. Nilsson MR and Raleigh DP, J. Mol. Biol, 1999, 294, 1375–1385. [PubMed: 10600392]
19. Westermark P, Engström U, Johnson KH, Westermark GT and Betsholtz C, Proc. Natl. Acad. Sci. U. S. A, 1990, 87, 5036–5040. [PubMed: 2195544]
20. Goldsbury C, Goldie K, Pellaud J, Seelig J, Frey P, Müller SA, Kistler J, Cooper GJ and Aebi U, J. Struct. Biol, 2000, 130, 352–362. [PubMed: 10940238]
21. Tenidis K, Waldner M, Bernhagen J, Fischle W, Bergmann M, Weber M, Merkle ML, Voelter W, Brunner H and Kapurniotu A, J. Mol. Biol, 2000, 295, 1055–1071. [PubMed: 10656810]
22. Hoffmann W, Folmert K, Moschner J, Huang X, von Berlepsch H, Koksch B, Bowers MT, von Helden G and Pagel K, J. Am. Chem. Soc, 2018, 140, 244–249. [PubMed: 29235867]
23. Tatarek-Nossol M, Yan LM, Schmauder A, Tenidis K, Westermark G and Kapurniotu A, Chem. Biol, 2005, 12, 797–809. [PubMed: 16039527]
24. Wu C, Lei H and Duan Y, Biophys. J, 2004, 87, 3000–3009. [PubMed: 15326028]
25. Sarkar D, Chakraborty I, Condorelli M, Ghosh B, Mass T, Weingarth M, Mandal AK, La Rosa C, Subramanian V and Bhunia A, ChemMedChem, 2020, 15, 293–301. [PubMed: 31762186]
26. Gupta A, Dey S, Bhowmik D and Maiti S, J. Phys. Chem. B, 2022, 126, 1016–1023. [PubMed: 35104126]
27. Miyazato M, Nakazato M, Shiomi K, Aburaya J, Kangawa K, Matsuo H and Matsukura S, Diabetes Res. Clin. Pract, 1992, 15, 31–36. [PubMed: 1541233]
28. Wang W, Nema S and Teagarden D, Int. J. Pharm, 2010, 390, 89–99. [PubMed: 20188160]
29. Yoshimura Y, Lin Y, Yagi H, Lee YH, Kitayama H, Sakurai K, So M, Ogi H, Naiki H and Goto Y, Proc. Natl. Acad. Sci. U. S. A, 2012, 109, 14446–14451. [PubMed: 22908252]

30. Chakraborty I, Kar RK, Sarkar D, Kumar S, Maiti NC, Mandal AK and Bhunia A, ACS Chem. Neurosci, 2021, 12, 2903–2916. [PubMed: 34292711]
31. Zhang J, Tan J, Pei R and Ye S, Langmuir, 2020, 36, 1530–1537. [PubMed: 31995712]
32. Brender JR, Hartman K, Nanga RP, Popovych N, de la Salud Bea R, Vivekanandan S, Marsh EN and Ramamoorthy A, J. Am. Chem. Soc, 2010, 132, 8973–8983. [PubMed: 20536124]
33. Klement K, Wieligmann K, Meinhardt J, Hortschansky P, Richter W and Fändrich M, J. Mol. Biol, 2007, 373, 1321–1333. [PubMed: 17905305]
34. Bera S, Gayen N, Mohid SA, Bhattacharyya D, Krishnamoorthy J, Sarkar D, Choi J, Sahoo N, Mandal AK, Lee D and Bhunia A, ACS Chem. Neurosci, 2020, 11, 1965–1977. [PubMed: 32492332]
35. van Dijk E, Hoogeveen A and Abeln S, PLoS Comput. Biol, 2015, 11, e1004277. [PubMed: 26000449]
36. Camilloni C, Bonetti D, Morrone A, Giri R, Dobson CM, Brunori M, Gianni S and Vendruscolo M, Sci. Rep, 2016, 6, 28285. [PubMed: 27461719]
37. Wei G, Su Z, Reynolds NP, Arosio P, Hamley IW, Gazit E and Mezzenga R, Chem. Soc. Rev, 2017, 46, 4661–4708. [PubMed: 28530745]
38. Bhattacharya M, Jain N and Mukhopadhyay S, J. Phys. Chem. B, 2011, 115, 4195–4205. [PubMed: 21417250]
39. Petkova AT, Leapman RD, Guo Z, Yau WM, Mattson MP and Tycko R, Science, 2005, 307, 262–265. [PubMed: 15653506]
40. Paravastu AK, Petkova AT and Tycko R, Biophys. J, 2006, 90, 4618–4629. [PubMed: 16565054]
41. Campioni S, Carret G, Jordens S, Nicoud L, Mezzenga R and Riek R, J. Am. Chem. Soc, 2014, 136, 2866–2875. [PubMed: 24460028]
42. Varnava KG, Mohid SA, Calligari P, Stella L, Reynison J, Bhunia A and Sarojini V, Bioconjugate Chem., 2019, 30, 1998–2010.
43. Biswas R, Das AR, Pradhan T, Touraud D, Kunz W and Mahiuddin S, J. Phys. Chem. B, 2008, 112, 6620–6628. [PubMed: 18457442]
44. Bhattacharyya D, Kumar R, Mehra S, Ghosh A, Maji SK and Bhunia A, Chem. Commun, 2018, 54, 3605–3608.
45. LeVine H, Methods Enzymol., 1999, 309, 274–284. [PubMed: 10507030]
46. Ratha BN, Ghosh A, Brender JR, Gayen N, Ilyas H, Neeraja C, Das KP, Mandal AK and Bhunia A, J. Biol. Chem, 2016, 291, 23545–23556. [PubMed: 27679488]
47. Mosmann T, J. Immunol. Methods, 1983, 65, 55–63. [PubMed: 6606682]
48. Tiiman A, Noormägi A, Friedemann M, Krishtal J, Palumaa P and Tõugu V, J. Pept. Sci, 2013, 19, 386–391. [PubMed: 23609985]
49. Meisl G, Kirkegaard JB, Arosio P, Michaels TC, Vendruscolo M, Dobson CM, Linse S and Knowles TP, Nat. Protoc, 2016, 11, 252–272. [PubMed: 26741409]
50. Xu Y, Maya-Martinez R, Guthertz N, Heath GR, Manfield IW, Breeze AL, Sobott F, Foster R and Radford SE, Nat. Commun, 2022, 13, 1040. [PubMed: 35210421]
51. Kusumoto Y, Lomakin A, Teplow DB and Benedek GB, Proc. Natl. Acad. Sci. U. S. A, 1998, 95, 12277–12282. [PubMed: 9770477]
52. Singh PK, Kumbhakar M, Pal H and Nath S, J. Phys. Chem. B, 2010, 114, 2541–2546. [PubMed: 20095597]
53. Stsiapura VI, Maskevich AA, Kuzmitsky VA, Uversky VN, Kuznetsova IM and Turoverov KK, J. Phys. Chem. B, 2008, 112, 15893–15902. [PubMed: 19367903]
54. Saha SK, Purkayastha P, Das AB and Dhara S, J. Photochem. Photobiol., A, 2008, 199, 179–187.
55. Sulatskaya AI, Maskevich AA, Kuznetsova IM, Uversky VN and Turoverov KK, PLoS One, 2010, 5, e15385. [PubMed: 21048945]
56. Singh PK, Kumbhakar M, Pal H and Nath S, Phys. Chem. Chem. Phys, 2011, 13, 8008–8014. [PubMed: 21445410]
57. Lakowicz JR, Principles of fluorescence spectroscopy, Springer, 2006.

58. Bharadwaj P, Solomon T, Sahoo BR, Ignasiak K, Gaskin S, Rowles J, Verdile G, Howard MJ, Bond CS, Ramamoorthy A, Martins RN and Newsholme P, Sci. Rep, 2020, 10, 10356. [PubMed: 32587390]
59. Jean L, Lee CF and Vaux DJ, Biophys. J, 2012, 102, 1154–1162. [PubMed: 22404938]
60. D'Amico M, Di Carlo MG, Groenning M, Militello V, Vetri V and Leone M, J. Phys. Chem. Lett, 2012, 3, 1596–1601. [PubMed: 26285714]
61. Tjernberg LO, Lilliehöök C, Callaway DJ, Näslund J, Hahne S, Thyberg J, Terenius L and Nordstedt C, J. Biol. Chem, 1997, 272, 12601–12605. [PubMed: 9139713]
62. Gordon DJ, Sciarretta KL and Meredith SC, Biochemistry, 2001, 40, 8237–8245. [PubMed: 11444969]
63. Scrocchi LA, Chen Y, Waschuk S, Wang F, Cheung S, Darabie AA, McLaurin J and Fraser PE, J. Mol. Biol, 2002, 318, 697–706. [PubMed: 12054816]
64. Ghosh A, Pithadia AS, Bhat J, Bera S, Midya A, Fierke CA, Ramamoorthy A and Bhunia A, Biochemistry, 2015, 54, 2249–2261. [PubMed: 25785896]
65. Akter R, Cao P, Noor H, Ridgway Z, Tu LH, Wang H, Wong AG, Zhang X, Abedini A, Schmidt AM and Raleigh DP, J. Diabetes Res, 2016, 2016, 2798269. [PubMed: 26649319]
66. Ulamec SM, Brockwell DJ and Radford SE, Front. Neurosci, 2020, 14, 611285. [PubMed: 33335475]
67. Brender JR, Lee EL, Cavitt MA, Gafni A, Steel DG and Ramamoorthy A, J. Am. Chem. Soc, 2008, 130, 6424–6429. [PubMed: 18444645]
68. Koo BW and Miranker AD, Protein Sci., 2005, 14, 231–239. [PubMed: 15576552]
69. Biancalana M and Koide S, Biochim. Biophys. Acta, 2010, 1804, 1405–1412. [PubMed: 20399286]
70. Ziaunys M, Sakalauskas A and Smirnovas V, Biomacromolecules, 2020, 21, 4989–4997. [PubMed: 33201685]
71. Sulatskaya AI, Rodina NP, Sulatsky MI, Povarova OI, Antifeeva IA, Kuznetsova IM and Turoverov KK, Int. J. Mol. Sci, 2018, 19, 2486.
72. Stefani M and Rigacci S, Int. J. Mol. Sci, 2013, 14, 12411–12457. [PubMed: 23765219]
73. Glabe CG, J. Biol. Chem, 2008, 283, 29639–29643. [PubMed: 18723507]
74. Lee SJ, Nam E, Lee HJ, Savelieff MG and Lim MH, Chem. Soc. Rev, 2017, 46, 310–323. [PubMed: 27878186]
75. Mannini B, Mulvihill E, Sgromo C, Cascella R, Khodarahmi R, Ramazzotti M, Dobson CM, Cecchi C and Chiti F, ACS Chem. Biol, 2014, 9, 2309–2317. [PubMed: 25079908]
76. Vaiana SM, Best RB, Yau WM, Eaton WA and Hofrichter J, Biophys. J, 2009, 97, 2948–2957. [PubMed: 19948124]

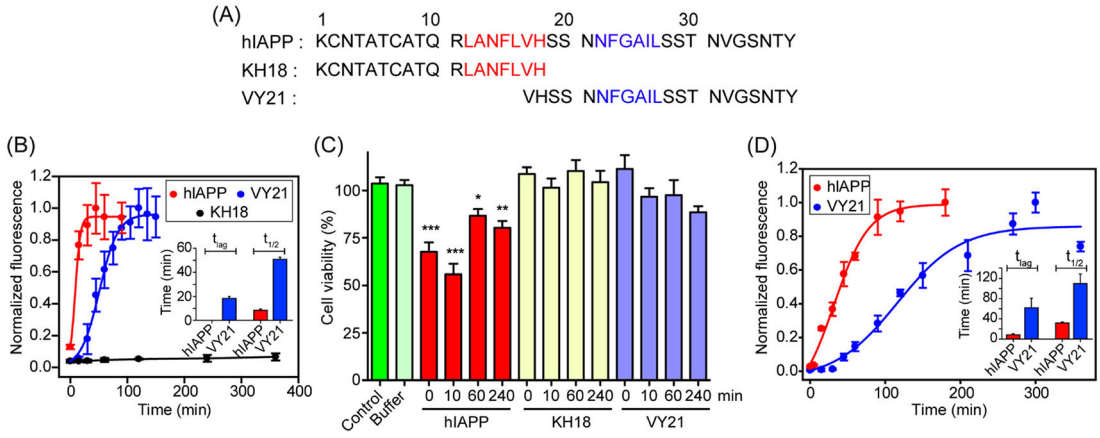

Fig. 1.

(A) Amino acid sequence of peptides under investigation with highlighted crucial motifs. (B) Aggregation kinetics of peptides investigated by ThT based fluorescence assay at 37 °C under shaking conditions (250 rpm). (C) RIN-5F cells were treated with hIAPP (10 μM), KH18 (10 μM) and VY21 (10 μM) for 24 h and cell viability was measured by MTT assay under shaking condition. Values are represented as mean ± SEM, $n = 9$. Significance was analysed using one-way ANOVA, $*p < 0.05$, $**p < 0.01$, $***p < 0.001$. (D) ThT fluorescence kinetics of hIAPP (red) and VY21 (blue), at 25 °C under shaking conditions (250 rpm). All kinetic curves were normalized with respect to hIAPP. Insets show the corresponding half-time ($t_{1/2}$) and lag-time (t_{lag}) of the aggregation kinetics obtained from Boltzmann fit. All experiments were repeated three times, and the data were averaged (±SD).

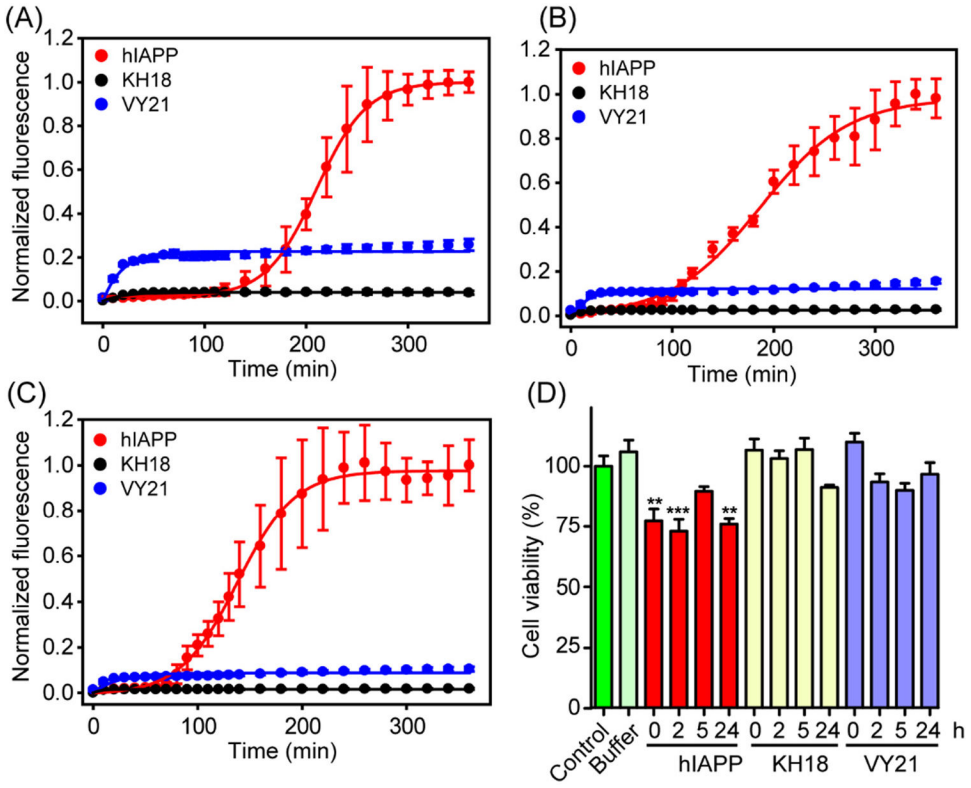

Fig. 2.

Aggregation kinetics of hIAPP (red), KH18 (black), and VY21 (blue) at under non-shaking condition (A) 25 °C, (B) 32 °C, and (C) 37 °C, monitored by ThT fluorescence. All experiments were repeated three times, and the data were averaged (±SD). (D) Cell viability was measured by incubating equimolar (10 μM) concentrations of indicated peptides generated at 25°, under non-shaking condition. Values are represented as mean ± SEM, $n = 6$. Significance was calculated using one-way ANOVA, $^{**}p < 0.01$, $^{***}p < 0.001$.

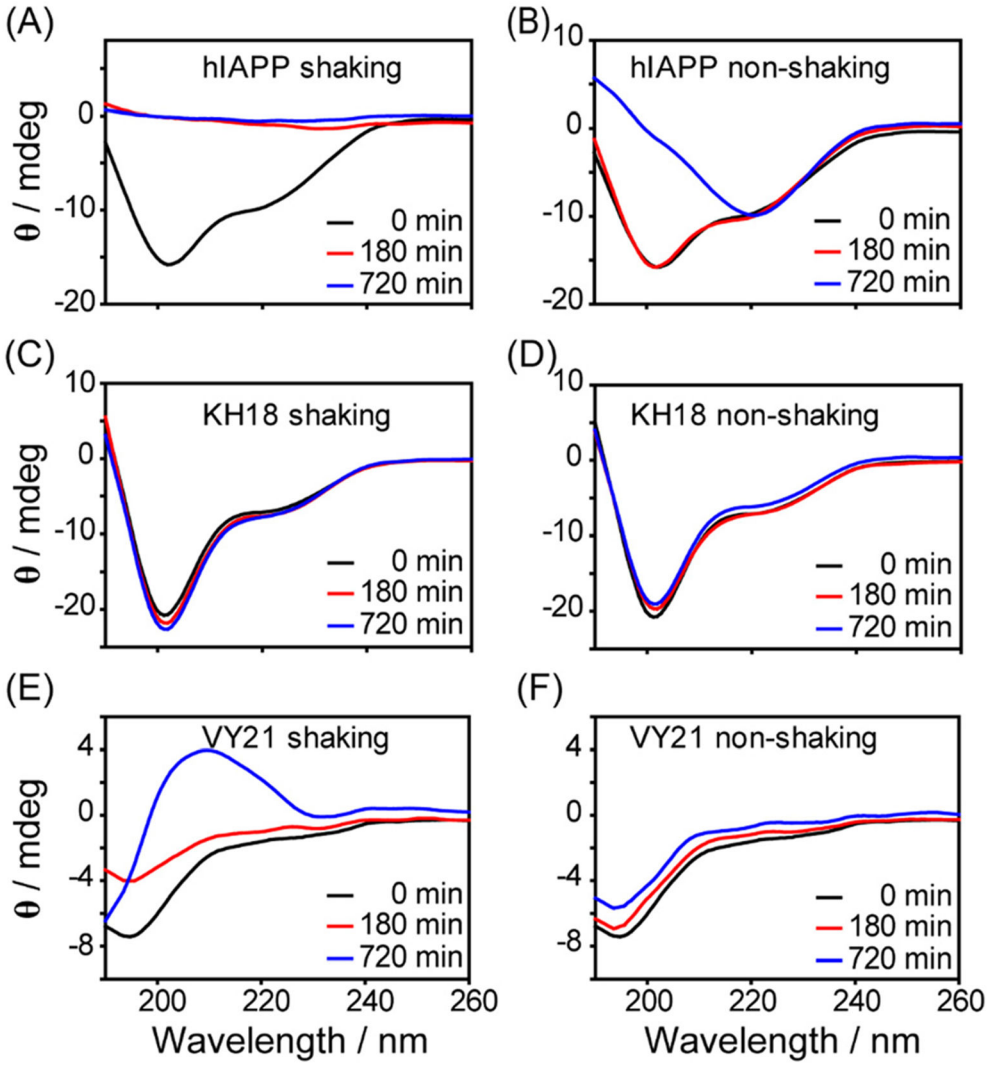

Fig. 3.

Monitoring secondary structural changes during aggregation by CD spectroscopy. Time-dependent CD spectra of (A) hIAPP, (C) KH18, and (E) VY21 at 37 °C under shaking conditions. Time-dependent CD spectra of (B) hIAPP, (D) KH18, and (F) VY21 at 25 °C under non-shaking conditions. All kinetic profiles are color coded.

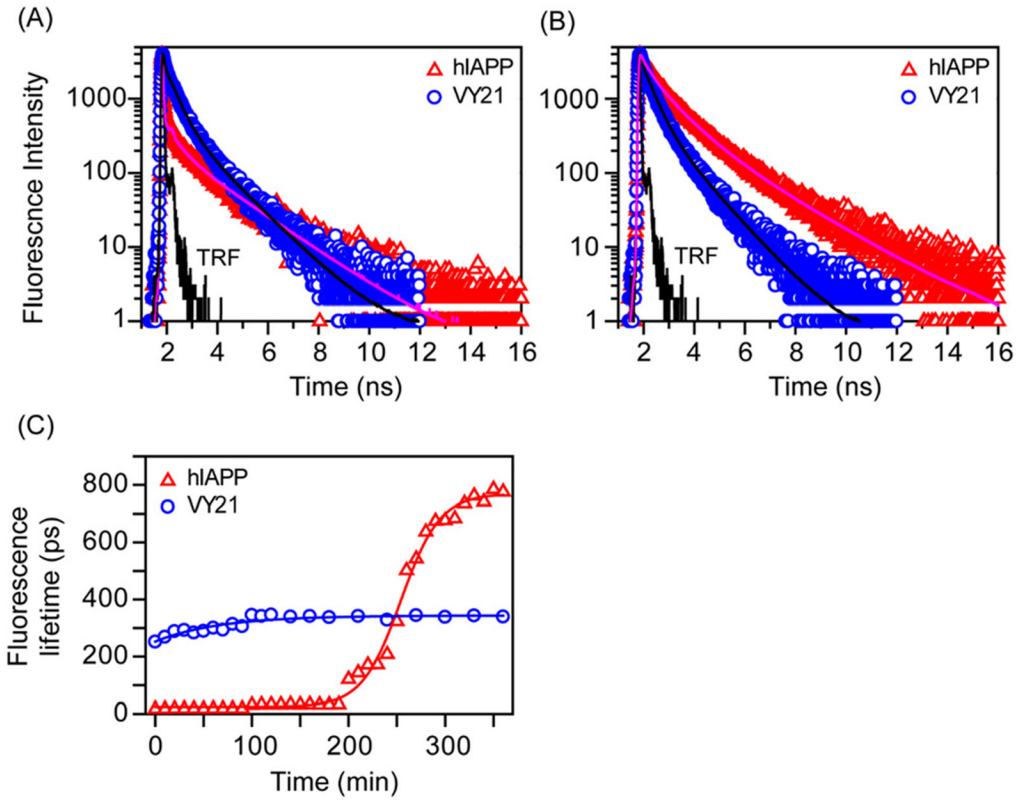

Fig. 4.

(A) Time-resolved fluorescence decay of ThT in presence of hIAPP (red) and VY21 (blue) at 0 min and (B) after 360 min of incubation at 25 °C under non-shaking conditions. (C) Time-resolved fluorescence lifetime kinetics of ThT in presence of hIAPP (red), and VY21 (blue).

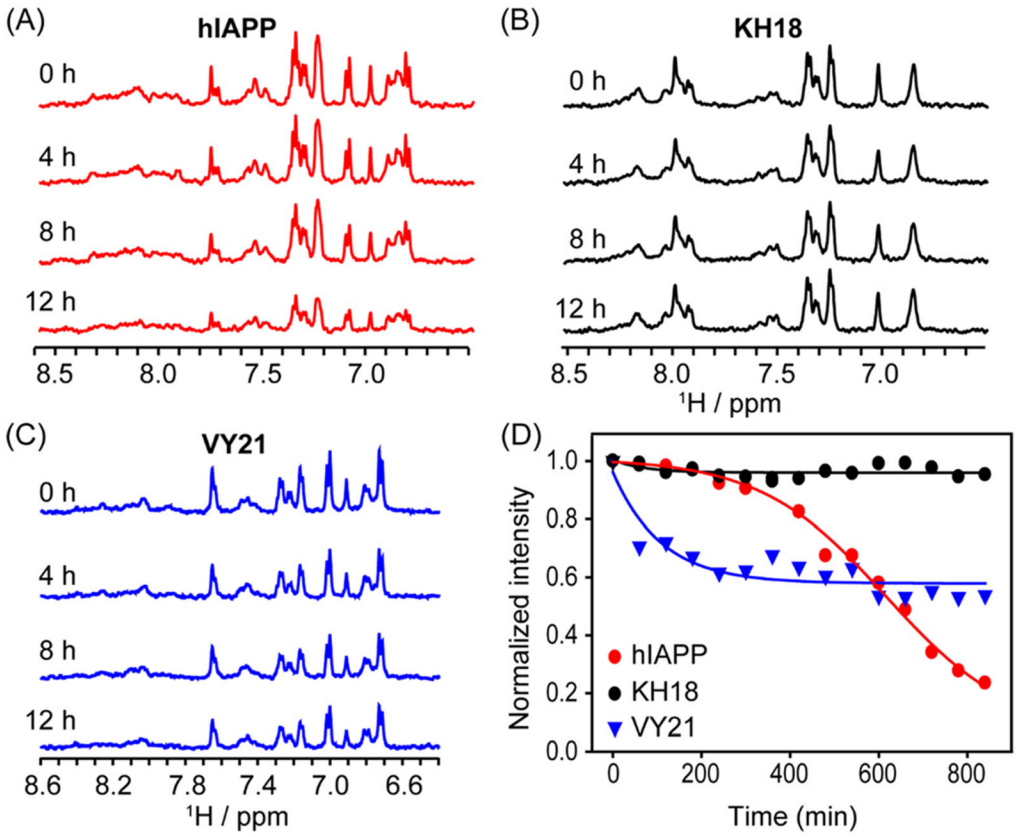

Fig. 5.

Time-dependent ^{1}D NMR spectra of (A) hIAPP, (B) KH18, (C) VY21 at 25 °C under non-shaking conditions. (D) ^{1}H NMR intensity decay kinetics of hIAPP (red), KH18 (black), and VY21 (blue). All kinetic profiles are color coded.

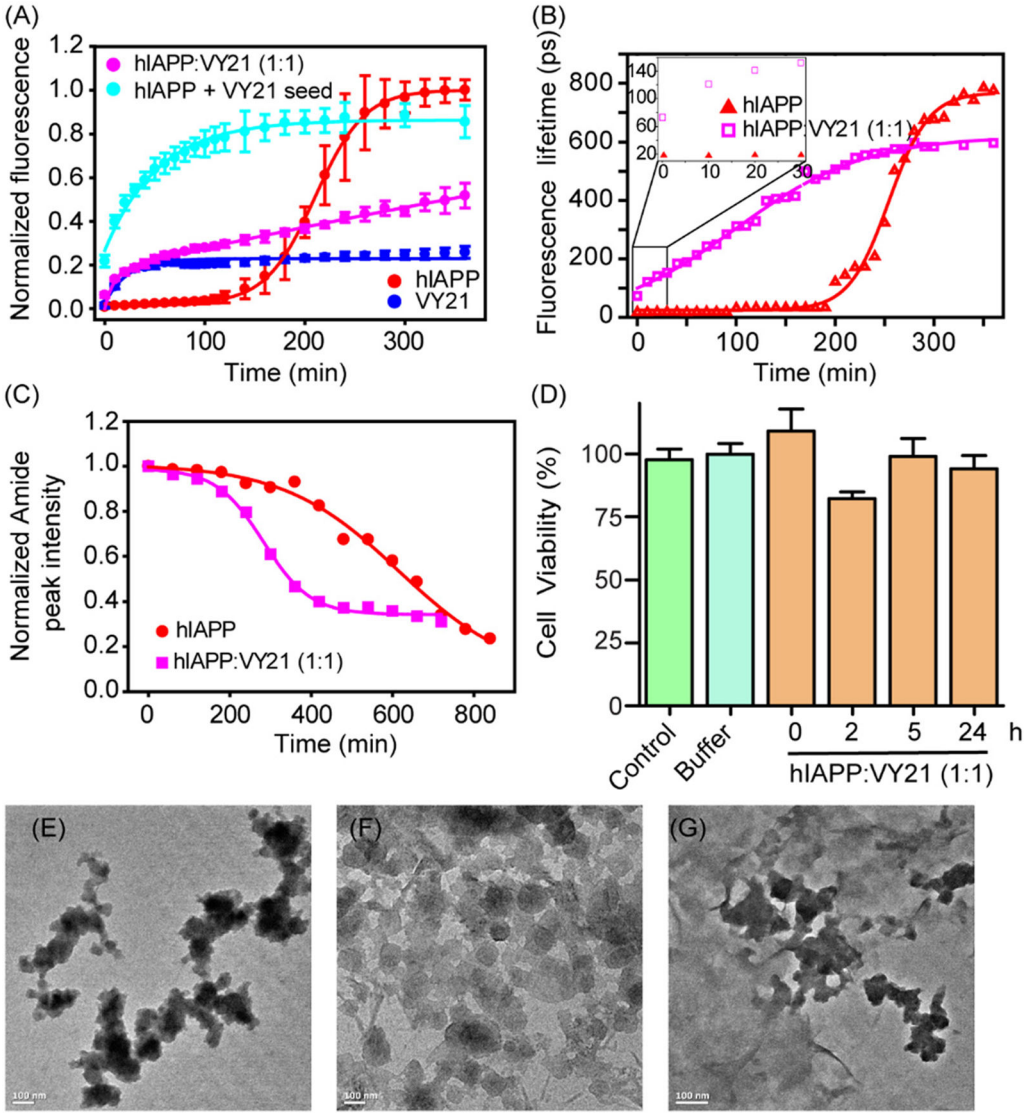

Fig. 6.

(A) ThT fluorescence kinetics of hIAPP (red), VY21 (blue), hIAPP co-incubated with VY21 at a 1 : 1 molar ratio aggregates (pink), and hIAPP after addition of VY21 oligomers (cyan). (B) Time-resolved fluorescence lifetime kinetics of ThT in presence of hIAPP (red), and hIAPP co-incubated with VY21 at a 1 : 1 molar ratio aggregates (pink). Inset highlights the initial time points. (C) ^{1}H NMR intensity decay kinetics of hIAPP with VY21 at a 1 : 1 molar ratio. (D) Cell viability was measured by incubating (10 μM) aggregated peptide generated from hIAPP co-incubated with VY21 at a 1 : 1 molar ratio. Values are represented as mean ± SEM, $n = 6$. TEM images of (E) hIAPP, (F) VY21, and (G) hIAPP co-incubated with VY21 at a 1 : 1 molar ratio aggregates. All experiments were done at 25 °C, under non-shaking conditions.

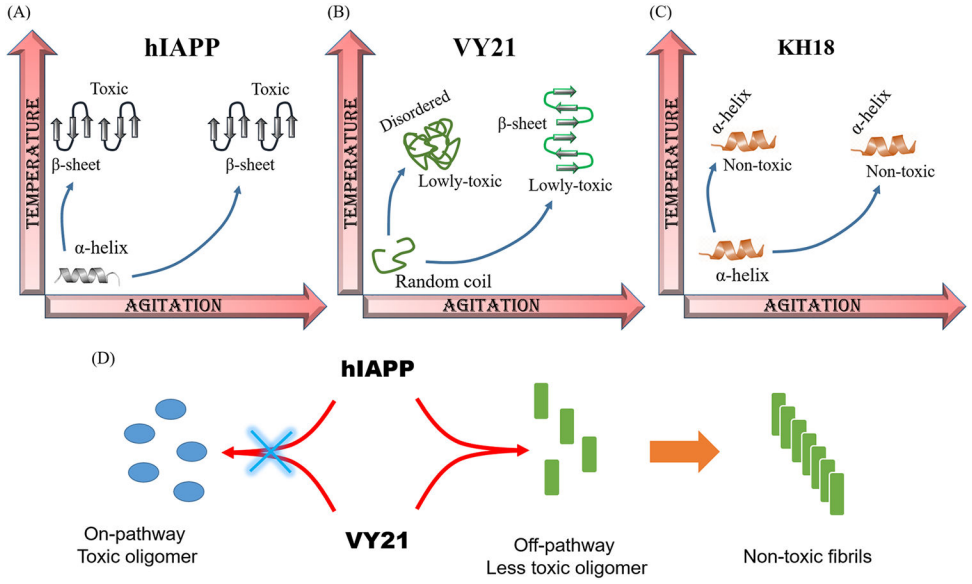

Fig. 7.

Schematic representation illustrating effect of temperature and agitation on the self-assembly of hIAPP, VY21, and KH18. (A) hIAPP undergoes fibrillation under different temperature and agitation conditions, generating toxic fibrils. (B) VY21 can evolve into either disordered oligomers under non-shaking conditions or ordered fibrils under shaking conditions at different temperatures, both cases generating less toxic species. (C) KH18 remains in helical conformation even at elevated temperature and shaking conditions and are non-toxic in nature. (D) VY21 reduces the presence of toxic hIAPP oligomers by altering the hIAPP fibrillation kinetics which drastically increases the formation of non-toxic fibrils.